



HAL
open science

Four new planetesimals around typical and pre-main-sequence stars (PLATYPUS) debris discs at 8.8 mm

Brodie J. Norfolk, Sarah T. Maddison, Jonathan P. Marshall, Grant M. Kennedy, Gaspard Duchêne, David J. Wilner, Christophe Pinte, Attila Moór, Brenda Matthews, Péter Ábrahám, et al.

► To cite this version:

Brodie J. Norfolk, Sarah T. Maddison, Jonathan P. Marshall, Grant M. Kennedy, Gaspard Duchêne, et al.. Four new planetesimals around typical and pre-main-sequence stars (PLATYPUS) debris discs at 8.8 mm. *Monthly Notices of the Royal Astronomical Society*, 2021, 507, pp.3139-3147. 10.1093/mnras/stab1901 . insu-03705262

HAL Id: insu-03705262

<https://insu.hal.science/insu-03705262>

Submitted on 6 Aug 2022

HAL is a multi-disciplinary open access archive for the deposit and dissemination of scientific research documents, whether they are published or not. The documents may come from teaching and research institutions in France or abroad, or from public or private research centers.

L'archive ouverte pluridisciplinaire **HAL**, est destinée au dépôt et à la diffusion de documents scientifiques de niveau recherche, publiés ou non, émanant des établissements d'enseignement et de recherche français ou étrangers, des laboratoires publics ou privés.

Four new planetesimals around typical and pre-main-sequence stars (PLATYPUS) debris discs at 8.8 mm

Brodie J. Norfolk,¹★ Sarah T. Maddison,¹ Jonathan P. Marshall,^{2,3} Grant M. Kennedy^{4,5},
Gaspard Duchêne,^{6,7} David J. Wilner,⁸ Christophe Pinte^{9,10}, Attila Moór,^{11,12} Brenda Matthews,^{13,14}
Péter Ábrahám,^{11,12} Ágnes Kóspál^{11,12,15} and Nienke van der Marel^{13,14}

¹Centre for Astrophysics and Supercomputing (CAS), Swinburne University of Technology, Hawthorn, VIC 3122, Australia

²Academia Sinica, Institute of Astronomy and Astrophysics, 11F Astronomy-Mathematics Building, NTU/AS campus, No. 1, Section 4, Roosevelt Rd., Taipei 10617, Taiwan

³Centre for Astrophysics, University of Southern Queensland, Toowoomba, QLD 4350, Australia

⁴Department of Physics, University of Warwick, Gibbet Hill Road, Coventry CV4 7AL, UK

⁵Centre for Exoplanets and Habitability, University of Warwick, Gibbet Hill Road, Coventry CV4 7AL, UK

⁶Astronomy Department, University of California, Berkeley, CA 94720, USA

⁷Université Grenoble Alpes / CNRS, Institut de Planétologie et d'Astrophysique de Grenoble, F-38000 Grenoble, France

⁸Harvard-Smithsonian Center for Astrophysics, 60 Garden Street, Cambridge, MA 02138, USA

⁹Monash Centre for Astrophysics (MoCA) and School of Physics and Astronomy, Monash University, Clayton, VIC 3800, Australia

¹⁰Univ. Grenoble Alpes, CNRS, IPAG, F-38000 Grenoble, France

¹¹Konkoly Observatory, Research Centre for Astronomy and Earth Sciences, Eötvös Loránd Research Network (ELKH), H-1121 Budapest, Konkoly-Thege Miklós út 15–17, Hungary

¹²ELTE Eötvös Loránd University, Institute of Physics, Pázmány Péter sétány 1/A, 1117 Budapest, Hungary

¹³Department of Physics & Astronomy, University of Victoria, Victoria, BC V8P 5C2, Canada

¹⁴Herzberg Astronomy & Astrophysics Programs, National Research Council of Canada, 5071 West Saanich Road, Victoria, BC V9E 2E7, Canada

¹⁵Max Planck Institute for Astronomy, Königstuhl 17, D-69117 Heidelberg, Germany

Accepted 2021 June 21. Received 2021 June 19; in original form 2021 May 24

ABSTRACT

Millimetre continuum observations of debris discs can provide insights into the physical and dynamical properties of the unseen planetesimals that these discs host. The material properties and collisional models of planetesimals leave their signature on the grain size distribution, which can be traced through the millimetre spectral index. We present 8.8 mm observations of the debris discs HD 48370, CPD-72 2713, HD 131488, and HD 32297 using the Australian Telescope Compact Array (ATCA) as part of the PLanetesimals Around TYpical Pre-main-seqUence Stars (PLATYPUS) survey. We detect all four targets with a characteristic beam size of 5 arcsec and derive a grain size distribution parameter that is consistent with collisional cascade models and theoretical predictions for parent planetesimal bodies where binding is dominated by self-gravity. We combine our sample with 19 other millimetre-wavelength-detected debris discs from the literature and calculate a weighted mean grain size power-law index that is close to analytical predictions for a classical steady-state collisional cascade model. We suggest the possibility of two distributions of q in our debris disc sample; a broad distribution (where $q \sim 3.2\text{--}3.7$) for ‘typical’ debris discs (gas-poor/non-detection), and a narrow distribution (where $q < 3.2$) for bright gas-rich discs. Or alternatively, we suggest that there exists an observational bias between the grain size distribution parameter and absolute flux that may be attributed to the detection rates of faint debris discs at $\sim\text{cm}$ wavelengths.

Key words: techniques: interferometric – planets and satellites: dynamical evolution and stability – circumstellar matter – planetary systems.

1 INTRODUCTION

Debris discs are the final stage of protoplanetary disc evolution (Williams & Cieza 2011; Wyatt et al. 2015). The majority of primordial gas has either accreted on to the star/companions or been blown away by photoevaporative winds, and the remaining dust

is replenished through ongoing collisions between dust-producing planetesimals, i.e. asteroids and comets (Wyatt 2008; Matthews et al. 2014).

Collisions in the disc are driven by planetesimal stirring that is triggered by either the interaction with smaller bodies that excite the belt (Kenyon & Bromley 2002, 2008; Krivov & Booth 2018), or by the dynamical influence of fully formed planets (Mustill & Wyatt 2009). The size distribution of the grains produced by these collisions provides insight into the different physical and dynamical properties

* E-mail: brodiejamesnorfolk@gmail.com

Table 1. Stellar properties of our four new PLATYPUS sources.

Source	RA	Dec.	Distance (pc)	SpType	Age (Myr)
HD 48370	06:43:01	−02:53:19	36.07 ± 0.07	G8	20–50
CPD-72 2713	22:42:48	−71:42:21	36.66 ± 0.03	K7-M0	24
HD 131488	14:55:08	−41:07:13	155 ± 2	A1	15
HD 32297	05:02:27	+07:27:39	133 ± 1	A5-A6	15-45

of the invisible parent planetesimals. The original collisional cascade model was formulated by Dohnanyi (1969), who used a power-law grain size distribution $dn(a) \propto a^{-q} da$, and determined $q = 3.5$ for grains with constant tensile strength and velocity dispersion. More recently, this standard model has been improved upon to include grain-size-dependant tensile strengths (Pan & Sari 2005) and velocity distributions (Pan & Schlichting 2012; Gáspár et al. 2012a) that result in a range of the grain size distribution exponent q between 3 and 4. This theoretically estimated range of q is supported by a number of millimetre wavelength observations (Ricci et al. 2012, 2015b; MacGregor et al. 2016; Marshall et al. 2017; Wilner et al. 2018; Moór et al. 2020). To date, numerical modelling of observations has constrained the parameter to $3.2 < q < 3.8$ for various grain materials (Hughes, Duchêne & Matthews 2018; Löhne 2020).

The underlying properties of parent planetesimals remains unknown. Observing multiple discs across a range of spectral types and ages can help address this. To further constrain the material properties of dusty debris discs, multiwavelength observations in the millimetre regime are required to determine the millimetre spectral index, α_{mm} (Beckwith et al. 1990; Gáspár et al. 2012a). α_{mm} is a function of the dust emissivity and can be used to constrain the collisional state of the disc (Krivov 2010; Ricci et al. 2012, 2015b). Despite their faint emission, observing at longer wavelengths (~ 1 cm) provides a better constraint on the mm spectral index (a long lever arm) and is effectively in the Rayleigh–Jeans regime for typical disc temperatures. Here, we present new results from PLANETESIMALS AROUND TYPICAL PRE-MAIN-SEQUENCE STARS (PLATYPUS), an ongoing survey of debris discs at 8.8 mm with the Australian Telescope Compact Array (ATCA; Ricci et al. 2015b; Marshall et al. 2017). The targets in this work are four relatively young debris disc host stars spanning a broad range of stellar luminosities that, including sources from the previously largest disc comparison survey (Löhne 2020), increases the number of systems with measured values to 22.

2 THE SAMPLE

The PLATYPUS sample are selected to have (1) declinations below 20° in order to be observable with the ATCA array, (2) complementary ALMA observations at 1.3 mm, and (3) are relatively compact to maximize surface brightness sensitivity. In this work, we add an additional four debris discs not previously observed at long wavelengths that span a range of spectral types and are comparatively young (50 Myr or less). We summarize the relevant stellar properties of the four sources in Table 1.

2.1 HD 48370

HD 48370 is a G8 V star (Torres et al. 2008) at a distance of 36.07 ± 0.07 pc (Gaia Collaboration 2018) and has an estimated age of ~ 20 –50 Myr (Torres et al. 2008). A peak radius for the disc to be at ~ 90 au using spatially resolved *Herschel* images (Moór et al. 2016; Marshall et al. 2021). Using archival 1.3 mm ALMA observations (Project ID: 2016.2.00200S) of HD 48370, we fit a simple Gaussian

to the observatory-calibrated visibilities and derive an integrated flux of 5.0 ± 0.5 mJy.

2.2 CPD-72 2713

CPD-72 2713 (CPD-72) is a late-type star with a derived spectral type of K7–M0 (Torres et al. 2006; Pecaú & Mamajek 2013; Gaidos et al. 2014). It resides at a distance of 36.66 ± 0.03 pc (Gaia Collaboration 2018) and is a member of the ≈ 24 Myr old β Pic moving group (Torres et al. 2006; Bell, Mamajek & Naylor 2015; Gagné et al. 2018; Lee & Song 2018). With new 1.33 mm ALMA observations, Moór et al. (2020) estimates the outer radius of the cold debris disc surrounding the host star to be 140 ± 14 au.

2.3 HD 131488

HD 131488 is an A2-type star (Melis et al. 2013) residing at a distance of 155 ± 2 pc (Gaia Collaboration 2018) and is ~ 15 Myr old (Mamajek, Meyer & Liebert 2002; Pecaú, Mamajek & Bubar 2012). It is a member of the Upper Centaurus Lupus moving group in the Sco–Cen association (Rizzuto, Ireland & Robertson 2011). By analysing spatially resolved ALMA continuum observations, Moór et al. (2017) derived a disc radius of $\sim 0'.57$ (~ 88 au). They also found that the disc harbours a substantial amount of CO gas ($\sim 0.1 M_{\oplus}$, considering the *Gaia* DR2 based distance of the object).

2.4 HD 32297

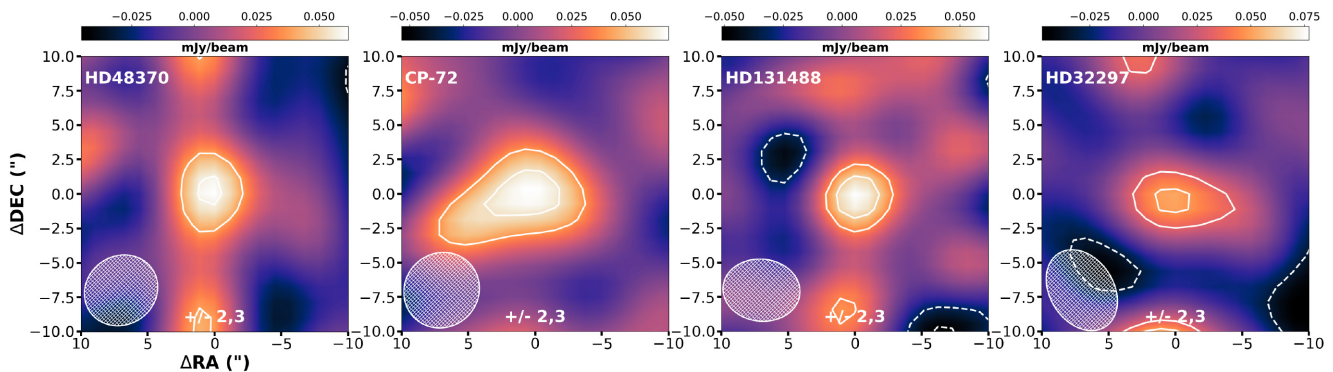
HD 32297 is an A5 V or A6 V-type star (Debes, Weinberger & Kuchner 2009) at a distance of 133 ± 1 pc (Gaia Collaboration 2018). Kalas (2005) estimates an age less than 30 Myr, whereas Esposito et al. (2020) derived a range of 15–45 Myr. MacGregor et al. (2018) fit the visibilities of high resolution 1.3 mm ALMA observations and derive the inner edge of the planetesimal belt to be 76 ± 8 au and the inner edge of the disc halo to be 122 ± 3 au, in agreement with previous Keck/NIRC2 imaging (Currie et al. 2012). They also constrain the outer edge of the halo to 440 ± 32 au, closely matching estimates from *HST* images (Schneider, Silverstone & Hines 2005). Duchêne et al. (2020) found the disc to be extremely symmetric in scattered light, with disc morphology in reasonable agreement with the ALMA results from MacGregor et al. (2018). HD 32297 is considered a CO-rich disc (Greaves et al. 2016) with a mass of $7.4 \times 10^{-2} M_{\oplus}$. This is the second most massive after HD131488, see MacGregor et al. (2018) and Moór et al. (2019), and is one of four CO-rich debris discs around ~ 30 –40 Myr A-type stars found to date, joining HD 21997 (Moór et al. 2011) and 49 Ceti (Zuckerman & Song 2012).

3 ATCA OBSERVATIONS AND DATA REDUCTION

We used the ATCA radio telescope to conduct our survey at 34 GHz (project code C2694, PI: Maddison). The Compact Array Broadband Backend (Wilson et al. 2011) provides observations with two bands that contain 2048×1 MHz channels, which we centred at 33 and 35 GHz. Observations were conducted in the hybrid H214 array configuration with antenna 6 flagged due to the increased phase noise on long baselines. This sets an effective baseline range from 92 to 247 m. The synthesized beam for each observation is detailed in Table 2. The weather during the observations varied for each science target, and the seeing monitor RMS path-length noise for each observation is summarized in Table 2.

Table 2. PLATYPUS survey results and observing log.

Source	Flux density (μJy)	1σ (μJy)	θ_{beam} (" \times ")	Date	Obs. time (min)	Band-pass	Calibrators flux	Gain/phase	Ave. path length rms (μm)
HD 48370	70.0	10.8	5.61 x 5.01	2019 Mar 01-02	225	1253-055	1934-638	0639-032	255
CPD-72 2713	95.9	16.1	5.74 x 5.40	2019 Mar 02	225	1921-293	1934-638	2229-6910	329
HD 131488	59.5	12.4	5.78 x 4.51	2019 Mar 02	430	1253-055	1934-638	1451-400	111
HD 32297	56.2	16.7	6.37 x 4.73	2019 Mar 01-02	450	0003-066	1934-638	0454+066	282


Figure 1. Images of the four debris discs detected in our 8.8-mm ATCA observations. The orientation is north up, east left. The synthesized ATCA beam FWHM extent and orientation for each observations is represented by the shaded ellipse in the bottom left of each panel. Contours are ± 2 and 3σ , with negative contours denoted by the dashed lines.

The science targets were observed with a repeated sequence of 10 min on-source integration and 2 min integration of the gain/phase calibrator. The bandpass and flux calibrators were observed for ~ 15 min and pointing checks were made on the phase calibrator every ~ 60 – 90 min. All observational and calibration details are summarized in Table 2.

The data were processed using the software package MIRIAD (Sault, Teuben & Wright 1995) and followed the standard procedure that involved: correcting for the frequency-dependent gain using the MIRIAD task *mfcal*; then using the flux density of the ATCA primary flux calibrator, 1937-638, to re-scale the visibilities measured by the correlator using the miriad task *mfcal* with the option *nopassol* set; and correcting for the gain of the system’s time variable properties due to changing conditions using the MIRIAD task *gpcal*. To reduce the noise in our data while maintaining as complete an observational track as possible, we flagged all data with a seeing monitor RMS path-length noise above $400 \mu\text{m}$ using *uvflag*, and calibrator amplitude readings that deviated more than 10 per cent from the mean flux using *blflag*. Any unusual spikes seen in the channel versus amplitude or the channel versus phase plots were also flagged using *uvflag*. We adopt a 10 per cent uncertainty on the absolute flux scale for our ATCA observations that is typical at these wavelengths (Ubach et al. 2012), and in agreement with the variations we observe of the gain calibrator flux.

After calibrating the data, images at 34 GHz were produced using robust weighting of 2 to achieve natural weighting and retain maximum detectable flux. The dirty images were cleaned to 5σ (five times the RMS noise level) using the *clean* task and the beam was restored using the *restor* task. The resulting images for our four sources are presented in Fig. 1. HD 48370, HD 131488, and HD 32297 exhibit a north–south alignment of residual emission peaks. This is an artefact from clean due to poorly sampling in *uv*-space. Given the marginal detection ($\sim 3\sigma$) and beam size with respect to the 3σ contours, the discs are consistent with being

unresolved and the flux density is calculated using the *imfit* task (Table 2) with the *source* parameter set to ‘point’. This fits a Gaussian with a width equal to the point spread function. We are unable to confirm the presence of stellar emission in our detections. To check for other forms of long-wavelength emission in our sources, either resolved observations or temporal monitoring is required (Ubach et al. 2017). However, there was a lack of strong, short (< 15 min) flares that would present as obvious deviations in the amplitude versus time relation for each target.

4 RESULTS

4.1 Spectral energy distributions

We combine our four newly acquired ATCA 8.8 mm flux measurements with photometry from the literature to derive flux density distributions (see Fig. 2). The photometry comes from a wide variety of sources, including Stömgren *uvby* (Paunzen 2015), *Gaia* (Gaia Collaboration 2018), 2MASS (Cutri et al. 2012), *WISE* (Wright et al. 2010), *Herschel* PACS (Sibthorpe et al. 2018, using our own PSF photometry), and various (sub-)mm papers (see Table 3 for references). We then simultaneously fit stellar and disc components as described by Yelverton et al. (2019); we use PHOENIX models (Allard, Homeier & Freytag 2012) for the stellar photosphere component, and a ‘modified’ blackbody function for the disc. The modified blackbody is simply a normal *Planck* function $B_\nu(T)$ where the emission is blackbody-like and is multiplied by an additional factor $(\lambda_0/\lambda)^{-\beta}$ beyond a fitted ‘break’ wavelength λ_0 where the slope becomes steeper. The spectral slope at long wavelengths (i.e. beyond λ_0) is therefore $2 - \beta$. Where a significantly better fit is found, two disc components are used (e.g. Chen et al. 2009; Kennedy & Wyatt 2014), though here we are focused on the parameters of the cooler component which contributes to the sub-mm and mm flux. The best-fitting models for HD 48370 and CPD-72 suggest a single dust belt

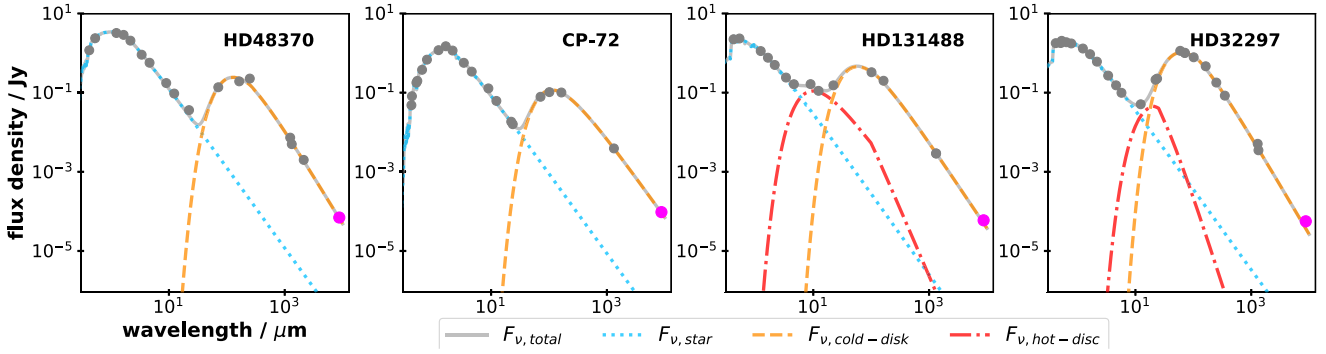


Figure 2. The spectral energy distributions of our four PLATYPUS debris discs. The magenta marker denotes the ATCA 8.8 mm flux, and the grey markers represent fluxes from the literature. The circle markers indicate detections above 3σ . The total flux, stellar photosphere, cold disc emission, and hot disc emission are represented by a hard grey line, blue-dotted line, orange-dashed line, and dash-dotted red line, respectively.

Table 3. The complete debris disc sample with sub-mm to mm observations. Our four new PLATYPUS sources with ATCA 8.8 mm fluxes are in bold. $\lambda_{1,\text{mm}}$ and $\lambda_{2,\text{mm}}$ are the wavelengths used to calculate the millimetre spectral slope α_{mm} (flux densities are presented in Table A1). L_* and T_d (the dust temperature of the cold component) for our four new sources is derived from the SED modelling. α_{pl} and q are calculated using equations (1) and (2), respectively. This table has been adapted from Löhne (2020).

Source	L_* (L_\odot)	Ref.	$\lambda_{1,\text{mm}}$	$\lambda_{2,\text{mm}}$	α_{mm}	Ref.	T_d (K)	α_{pl}	q	Ref.
AU Mic	0.1	2	1.3	9.0	<2.46	2	26	1.87	<3.33	13
CPD-72 2713	0.19	1	1.3 ^a	8.9	1.95 ± 0.17	1	45	1.94 ± 0.12	3.01 ± 0.09	1
ϵ Eri	0.3	2	1.3	7.0	>2.39	9	26	1.87	>3.29	13
HD 61005	0.5	2	1.3	9.0	2.49 ± 0.08	2	30	1.89	3.33 ± 0.04	13
HD 48370	0.77	1	1.3 ^a	8.9	2.26 ± 0.14	1	39	1.93 ± 0.14	3.18 ± 0.08	1
HD 107146	1.0	2	1.25	7.0	2.55 ± 0.11	10	27	1.88	3.37 ± 0.06	13
HD 377	1.0	2	0.87	9.0	>2.39	2	42	1.92	>3.26	13
HD 105	1.2	3	0.87	9.0	2.41 ± 0.16	3	33	1.90	3.28 ± 0.09	13
q^1 Eri	1.2	2	0.87	7.0	2.94 ± 0.10	2	33	1.90	3.58 ± 0.06	13
HD 104860	1.4	2	1.3	9.0	3.08 ± 0.23	2	31	1.89	3.66 ± 0.13	13
HD 15115	3.3	2	1.3	9.0	2.75 ± 0.15	2	40	1.92	3.46 ± 0.08	13
HD 181327	3.3	2	1.3	7.0	2.38 ± 0.05	10	42	1.92	3.26 ± 0.03	13
HR 8799	5.4	4	1.3	9.0	2.41 ± 0.17	11	40	1.92	3.27 ± 0.10	11
η Crv	6.6	5	0.85	9.0	2.10 ± 0.07	5,12	38	1.91	3.11 ± 0.04	13
HD 32297	8.2	1	1.3 ^a	8.9	2.11 ± 0.22	1	82	1.97 ± 0.07	3.07 ± 0.12	1
HD 95086	8.6	2	1.3	7.0	2.41 ± 0.12	2	35	1.91	3.27 ± 0.07	13
β Pic	8.7	2	0.87	7.0	2.81 ± 0.10	10	49	1.93	3.49 ± 0.06	13
HD 131835	10.5	6	0.87	9.0	2.17 ± 0.13	12	56	1.94	3.13 ± 0.07	13
HD 131488	12.8	1	1.3 ^a	8.9	2.05 ± 0.17	1	87	1.97 ± 0.06	3.04 ± 0.09	1
Formalhaut	16	2	1.3	7.0	2.70 ± 0.17	2	50	1.93	3.43 ± 0.09	13
49 Ceti	20	2	0.85	9.0	2.76 ± 0.11	2	64	1.95	3.45 ± 0.06	13
HR 4796 A	27	7,8	0.85	9.0	$>2.73 \pm 0.10$	12	73	1.96	3.43 ± 0.06	13

Notes. ^a $\lambda_{1,\text{mm}}$ fluxes are taken from Moór et al. (2020; CPD-72), this work (HD 48370), MacGregor et al. (2018; HD32297), and Moór et al. (2017; HD 131488).

References (1) this work, (2) MacGregor et al. (2016), (3) Marshall et al. (2018), (4) Holland et al. (2017), (5) Marino et al. (2017), (6) Hung et al. (2015a; 7) Gerbaldi et al. (1999), (8) Gaia Collaboration (2016), Gaia Collaboration (2018), (9) MacGregor et al. (2015b), (10) Ricci et al. (2015b), (11) Wilner et al. (2018), (12) Marshall et al. (2017), and (13) Löhne (2020).

is present at 39 and 45 K, respectively, whereas for HD 131488 and HD 32297 warm and cold belts were required at 414 and 87 K, and 225 and 82 K, respectively. Our targets have fairly shallow mm-wave slopes, meaning that the fitted values of β are close to zero and λ_0 is essentially unconstrained. As a result, we do not quote the results for λ_0 in this manuscript. We assume a 10 per cent uncertainty on our derived temperatures, which is generous, albeit has a minimal effect on q and is contained within the flux errors associated with the spectral mm index.

4.2 Determining the grain size distribution parameter

We derive the power-law index of the dust grain distribution q in an identical fashion to MacGregor et al. (2016). Briefly, this involves calculating the slope of the Planck function, α_{pl} , for our 8.8 mm fluxes and the next longest wavelength, which for our sample is at 1.3 mm:

$$\alpha_{\text{pl}} = \left| \frac{\log(B_{\nu_1}/B_{\nu_2})}{\log(\nu_1/\nu_2)} \right|, \quad (1)$$

where B_ν is the *Planck* function at the dust temperature T_d [(taken as the fitted temperature of the cool disc component in the spectral energy distributions (SEDs))] and $\nu_{1,2}$ are the frequencies of our two longest wavelength observations. The mm spectral index can then be calculated via $\alpha_{\text{mm}} = |\log(F_{\nu_1}/F_{\nu_2})/\log(\nu_1/\nu_2)|$. Assuming both flux measurements are in the Rayleigh–Jeans limit, q is then derived through the relation:

$$q = \frac{\alpha_{\text{mm}} - \alpha_{\text{pl}}}{\beta_s} + 3. \quad (2)$$

Draine (2006) analytically derives the q – β relation (where q is referred to as p in the manuscript) for grains in protoplanetary discs where β_s is the dust opacity spectral index of small particles. This relationship is valid for values of q in the range of 3–4 that are typical for debris discs. The value of β_s is dependent on the assumed material composition of the dust. β_s can vary from 1.3 to 2 (Jaeger et al. 1994; Draine 2004), however, the variation in β_s is comparable to the uncertainties on q derived from our analysis. We therefore assume that our grains are composed of astronomical silicate where $\beta_s = 1.8$, consistent with many other debris disc studies (MacGregor et al. 2016; Marshall et al. 2017).

Table 3 presents q values for our four sources calculated using equation 2, along with 18 other debris discs from the literature (see the references in Table 3). Due to an over subtraction during the removal of stellar emission, MacGregor et al. (2016) estimates a lower limit for the disc emission in AU Mic. This results in a counterintuitive upper limit of the q value.

5 DISCUSSION

Fig. 3 shows the distribution of q for 22 debris discs, the largest sub-mm to mm comparison sample to date. We include both the spectral type and age in Fig. 3, and find slightly lower correlations between the q value and stellar properties in comparison to findings presented in MacGregor et al. (2016; for a slightly smaller sample of 15 debris discs). For our sample of 22 debris discs, there does not appear to be any correlation between age and the grain size power law. Separating our sample at 50 Myr (see Table A1 for target ages), a Kolmogorov–Smirnov (K–S) test estimates a probability of 62 per cent that these two populations are drawn from the same distribution. However, there is a tentative trend with spectral type (slightly weaker than that found by MacGregor et al. 2016). Separating our sample by A–F stars and G–(K–M) stars, a K–S test estimates a probability of 23 per cent that these two populations are drawn from the same distribution. This suggests that stars with later spectral types may exhibit shallower grain size distributions, as previously seen in Pawellek & Krivov (2015). However, since we increase the percentage of later type stars in our sample compared to MacGregor et al. (2016) and our correlation decreases, we suggest that as the later star debris disc sample becomes more populated it is likely that the trend between q and the spectral type will disappear. We also include q -value model predictions from Dohnanyi (1969), Pan & Sari (2005), Pan & Schlichting (2012), Gáspár et al. (2012b), and Schüppler et al. (2015) indicated by the various hatched regions in the plot. The weighted mean q value of the sample, $\langle q \rangle = 3.31 \pm 0.07$, is in close agreement with mean weighted values from previous studies analysing a subset of our sample; $\langle q \rangle = 3.42 \pm 0.07$ (Ricci et al. 2015b), $\langle q \rangle = 3.36 \pm 0.02$ (MacGregor et al. 2016), and $\langle q \rangle = 3.23 \pm 0.04$ (Marshall et al. 2017). These values of q closely align with numerical results from Schüppler et al. (2015) rather than the larger range (3.3–4.6) presented by Pawellek et al. (2014) from far-infrared excesses. The q values derived for our new ATCA

observations all fall within the range predicted by Pan & Sari (2005). This suggests that the colliding bodies in these discs have a lower tensile strength and clumping is dominated by self-gravity, resulting in a shallower size distribution. Recently, Löhne (2020) reviewed dust material approximations (β) and compared them with numerical results for a number of materials (Bohren & Huffman 1983; Wolf & Voshchinnikov 2004). They suggest that the inferred grain size distribution indexes from dust material approximations are underestimated. However, when comparing a single material, astronomical silicate, their numerical values for q (seen in their fig. 14) are contained within our errors in Fig. 3.

As expected, the addition of our four new sources to the catalogue of debris discs has little impact on the weighted mean q value. However, all four targets populate the lower range of q values seen to date. In Fig. 4, we present the grain size distribution as a function of the interpolated 1 mm flux (Fig. 4a) and the interpolated 1 mm flux scaled to 50 pc (Fig. 4b). Using the SCIPY.STATS.PEARSONR function, we find a moderate correlation between q and the interpolated flux with a Pearson coefficient of 0.57. After scaling by the distance, this trend is reversed and the correlation is weaker with a Pearson coefficient of -0.22 . The absence of discs in the lower right region of Fig. 4(a) can be attributed to that fact that targets with high fluxes and shallower mm-slopes are defined as protoplanetary discs that are not included in debris disc surveys (e.g. see α_{mm} values presented in Lommen et al. 2007; Norfolk et al. 2021).

For optically thin debris discs, the size distribution index is related to the physics of grain collisions that may be influenced by the presence of gas. Lieman-Sifry et al. (2016) found that CO-rich systems in their sample of 12 resolved debris discs contain grain sizes on lower end of the size distribution. There are eight CO-bearing debris discs in our sample: β Pic (Matrà et al. 2017a), Fomalhaut (Matrà et al. 2017b), η Crv (Marino et al. 2017), and HD 181327 (Marino et al. 2016) contain relatively small amounts of CO gas ($M_{\text{CO}} < 10^{-4}M_{\oplus}$, represented by the open triangles in Fig. 4), whereas 49 Ceti (Moór et al. 2019), HD 32297 (Moór et al. 2019), HD 131488 (Moór et al. 2017), and HD 131835 (Moór et al. 2015) are CO-rich ($M_{\text{CO}} > 0.01M_{\oplus}$, represented by the closed triangles in Fig. 4). However, we find no conclusive trend, although gas-rich systems have marginally lower q values than gas-poor discs. This could be the result of either a gas-rich debris system preventing blow out and retaining smaller grains via gas drag, or frequent grain collisions that give rise to excess gas as well as a cascade of small dust grains (Lieman-Sifry et al. 2016). After scaling the flux (Fig. 4b), it becomes apparent that there may exist two distributions of q in our sample. These include a broad distribution (for $q \sim 3.2$ – 3.7) of q for ‘typical’ debris discs (gas-poor/non-detection) and a lower distribution (for $q < 3.2$) for bright gas-rich discs. To check this, we use a Fisher’s exact test on our data from Fig. 4b (a Fisher’s test exactly calculates the significance of there existing two distinct distributions in a sample). We first separate the groups at $q = 3.2$ and categorize the targets above and below 30 mJy (effectively separating our gas-rich discs and gas-poor/non-detection discs based on brightness), we obtain a significance of $p = 0.013$. If we instead categorize for gas-rich and gas-poor (which does not take the brightness into account), we obtain a lower significance of $p = 0.04$. Thus, there is some evidence that bright (in absolute terms) gas-rich debris discs tend to contain lower q values (the first test with $p = 0.013$). Or alternately given that our systems are faint in apparent flux, it is possible that an observational bias exists, especially since the Pearson coefficient becomes weaker once we scale the flux with the distance. For a fixed FIR/mm flux (e.g. the DUNES survey, Eiroa et al. 2013) the discs with the steepest size distribution will result

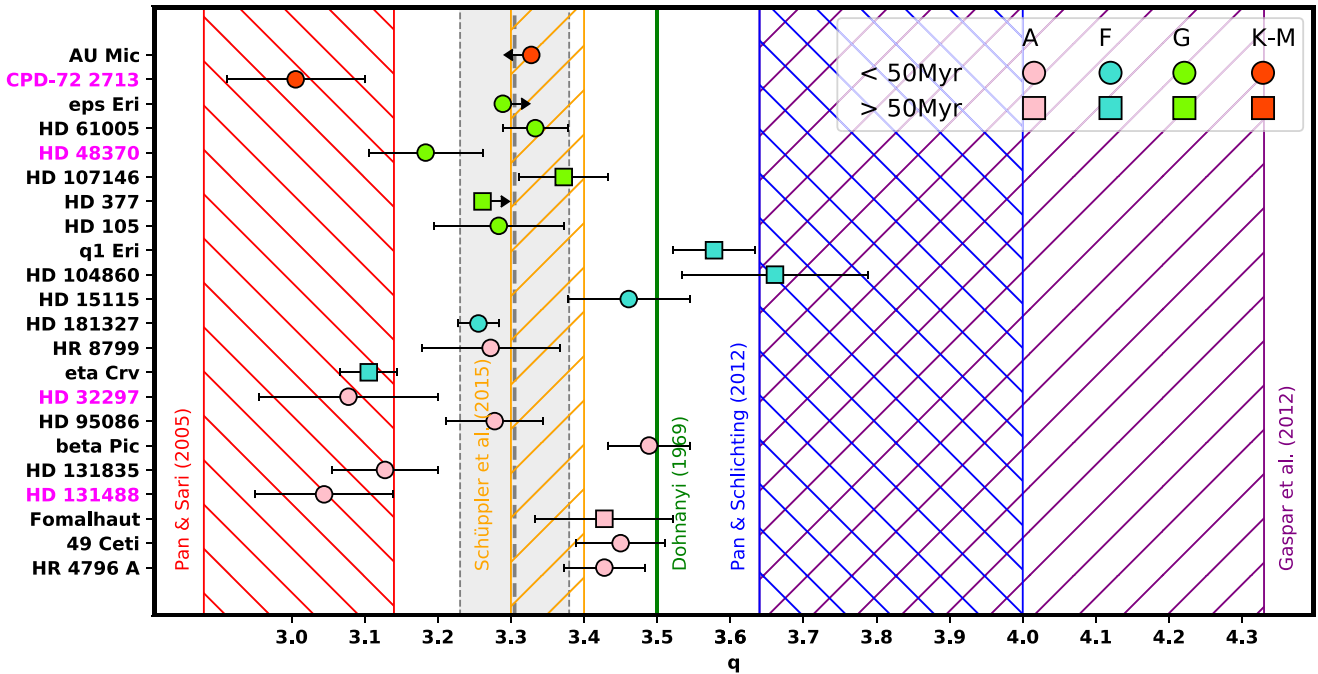


Figure 3. Distribution of grain size distribution power-law index q for the 22 debris discs. The labels for our four sources with new ATCA 8.8 mm flux are presented in magenta, while other sources are labelled in black as taken from Löhne (2020; see references within). The mean weighted q value and associated uncertainty ($\langle q \rangle = 3.31 \pm 0.07$) is shown by the grey region. Sources are ordered by their stellar luminosity from top to bottom (see Table 3 for specific luminosity values). The solid lines and dashed regions indicate different model predictions: ‘rubble pile’ planetesimals not dominated by material strength (Pan & Sari (2005); red), results of the ACE numerical model for AU Mic (Schüppler et al. (2015); yellow), the classic Dohnányi (1969) result (green), numerical results of Gáspár et al. (2012b; purple), and incorporating a size-dependent velocity distribution (Pan & Schlichting (2012); blue). The markers are differentiated by spectral type and age (see Table A1 for values and references). For spectral types A, F, G, and K–M the markers have colours red, green, blue, and pink, respectively. Targets with ages less than/greater than 50 Myr are represented by the circle/square markers, respectively.

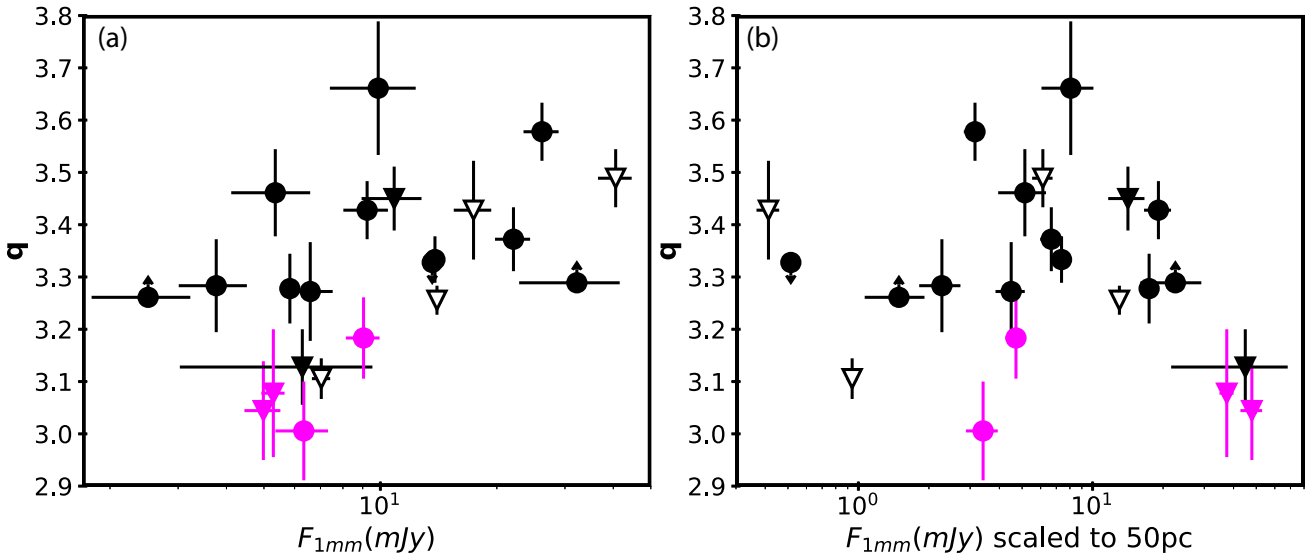


Figure 4. The grain size distribution parameter q as a function of (a) the interpolated 1 mm flux, and (b) the interpolated 1 mm flux scaled to a distance of 50 pc. Distances are taken from *Gaia* DR2 (Gaia Collaboration 2018). Our four new ATCA 8.8 mm sources are labelled by the magenta circles, and discs taken from the literature are labelled by the black circles. Gas-rich sources are represented by the closed triangles, and those that are gas-poor are represented by the open triangles. The Pearson correlation for this relation for (a) is 0.57 and for (b) is -0.22 .

in \sim cm fluxes that are below the detection limit. It is quite plausible that there exist many discs lurking below current sensitivity levels (Moro-Martín et al. 2015) and, as a result, the current mean weighted q value would be biased towards lower values. If there indeed does exist a population of lower q discs then the mean weighted grain size power-law index would shift closer towards the analytical models presented by Pan & Sari (2005; $2.88 < q < 3.14$) where colliding bodies are held together by self-gravity and contain relatively low tensile strengths.

6 CONCLUSIONS

In this work, we present new ATCA 8.8 mm observations of four debris discs and combine them to present the largest sample to date of 22 debris discs for which the grain size distribution power-law index q can be calculated to provide insights into the planetesimal populations in these discs. Our key findings are as follows:

(i) We present the longest wavelength observations to date of HD 48370, CPD-72 2713, HD 131488, and HD 32297 at 8.8 mm, and find that the q value of these sources are all quite low ($q < 3.2$), suggesting that the colliding bodies in these discs have a lower tensile strength and clumping is dominated by self-gravity.

(ii) For the entire sample of 22 debris discs, we evaluate a weighted mean value of the sample, $\langle q \rangle = 3.31$, consistent with analytical and numerical predictions for collisional cascade models.

(iii) With a larger sample (22 compared to 15 discs) we find that the tentative trend between q and the spectral type becomes weaker in comparison to findings from MacGregor et al. (2016).

(iv) We suggest possibility of two distributions of q ; a broad distribution (where $q \sim 3.2-3.7$) for ‘typical’ debris discs (gas-poor/non-detection), and a lower distribution (where $q < 3.2$) for bright gas-rich discs.

(v) Or alternatively, we suggest an observational bias may be present between the grain size distribution parameter and absolute flux, which is likely attributed to the detection rates of faint debris discs at \sim cm wavelengths.

Software: The MIRIAD package (Sault et al. 1995), PYTHON version 3.7, ASTROPY (Astropy Collaboration 2013, 2018), SCIPY (Virtanen et al. 2020), NUMPY (Harris et al. 2020), and MATPLOTLIB (Hunter 2007).

Facilities: Atacama Large Millimeter/sub-millimeter Array, ATCA.

ACKNOWLEDGEMENTS

The authors thank the referee for their constructive comments and suggestions. We thank Elodie Thilliez for useful discussions regarding our ATCA observing proposal. BJN is supported by an Australian Government Research Training Program Scholarship. GMK is supported by the Royal Society as a Royal Society University Research Fellow. JPM acknowledges research support by the Ministry of Science and Technology of Taiwan under grants MOST107-2119-M-001-031-MY3, MOST107-2119-M-001-031-MY3, and MOST109-2112-M-001-036-MY3, and Academia Sinica under grant AS-IA-106-M03. AM and PÁ acknowledge support from the grant KH-130526 of the Hungarian NKFIH. The Australia Telescope Compact Array is part of the Australia Telescope that is funded by the Commonwealth of Australia for operation as a National Facility managed by CSIRO. This research has used NASA’s Astrophysics Data System. The National Radio Astronomy Observatory is a facility of the National Science Foundation operated under agreement

by the Associated Universities, Inc. ALMA is a partnership of ESO (representing its member states), NSF (USA) and NINS (Japan), together with NRC (Canada) and NSC and ASIAA (Taiwan) and KASI (Republic of Korea), in cooperation with the Republic of Chile. The Joint ALMA Observatory is operated by ESO, AUI/NRAO, and NAOJ. This paper uses the following ALMA data: ADS/JAO.ALMA#2016.2.00200S.

DATA AVAILABILITY

The ATCA observational data used in this paper are available from the Australian National Telescope Facility Archive at <https://atoa.atnf.csiro.au> under project code C2696. The ALMA observational data are available from the ALMA science archive at <https://almascience.nrao.edu/aq/> under the project IDs listed in the Acknowledgements. Reduced observation data and models will be shared on reasonable request to the corresponding author.

REFERENCES

- Allard F., Homeier D., Freytag B., 2012, *Proc. IAU Symp.* 282, *From Interacting Binaries to Exoplanets: Essential Modeling Tools*. Kluwer, Dordrecht, p. 235
- Astropy Collaboration, 2013, *A&A*, 558, A33
- Astropy Collaboration, 2018, *AJ*, 156, 123
- Beckwith S. V. W., Sargent A. I., Chini R. S., Guenest R., 1990, *AJ*, 99, 924
- Bell C. P. M., Mamajek E. E., Naylor T., 2015, *MNRAS*, 454, 593
- Bohren C. F., Huffman D. R., 1983, *Absorption and Scattering of Light by Small Particles*. Wiley, New York
- Booth M. et al., 2017, *MNRAS*, 469, 3200
- Chen C. H., Sheehan P., Watson D. M., Manoj P., Najita J. R., 2009, *ApJ*, 701, 1367
- Choquet É. et al., 2016, *ApJ*, 817, L2
- Currie T. et al., 2012, *ApJ*, 757, 28
- Cutri R. M. et al., 2012, *VizieR Online Data Catalog*, II/281
- Debes J. H., Weinberger A. J., Kuchner M. J., 2009, *ApJ*, 702, 318
- Dent W. R. F. et al., 2014, *Science*, 343, 1490
- Dohnanyi J. S., 1969, *J. Geophys. Res.*, 74, 2531
- Draine B. T., 2004, in Blain A.W., Combes F., Draine B.T., Pflenniger D., Revaz Y., eds, *The Cold Universe*, Saas-Fee Advanced Course 32. Springer-Verlag, Berlin, p. 213
- Draine B. T., 2006, *ApJ*, 636, 1114
- Duchêne G. et al., 2020, *AJ*, 159, 251
- Eiroa C. et al., 2013, *A&A*, 555, A11
- Espósito T. M. et al., 2020, *AJ*, 160, 24
- Gagné J. et al., 2018, *ApJ*, 856, 23
- Gaia Collaboration, 2016, *A&A*, 595, A1
- Gaia Collaboration, 2018, *A&A*, 616, A1
- Gaidos E. et al., 2014, *MNRAS*, 443, 2561
- Gáspár A., Psaltis D., Özel F., Rieke G. H., Cooney A., 2012a, *ApJ*, 749, 14
- Gáspár A., Psaltis D., Rieke G. H., Özel F., 2012b, *ApJ*, 754, 74
- Gerbaldi M., Faraggiana R., Burnage R., Delmas F., Gómez A. E., Grenier S., 1999, *A&AS*, 137, 273
- Greaves J. S. et al., 2016, *MNRAS*, 461, 3910
- Harris C. R. et al., 2020, *Nature*, 585, 357–362
- Holland W. S. et al., 2003, *ApJ*, 582, 1141
- Holland W. S. et al., 2017, *MNRAS*, 470, 3606
- Hughes A. M. et al., 2017, *ApJ*, 839, 86
- Hughes A. M., Duchêne G., Matthews B. C., 2018, *ARA&A*, 56, 541
- Hung L.-W., Fitzgerald M. P., Chen C. H., Mittal T., Kalas P. G., Graham J. R., 2015a, *ApJ*, 802, 138
- Hung L.-W. et al., 2015b, *ApJ*, 815, L14
- Hunter J. D., 2007, *Comput. Sci. Eng.*, 9, 90
- Jaeger C., Mutschke H., Begemann B., Dorschner J., Henning T., 1994, *A&A*, 292, 641
- Kalas P., 2005, *ApJ*, 635, L169

- Kennedy G. M., Wyatt M. C., 2014, *MNRAS*, 444, 3164
- Kennedy G. M., Marino S., Matrà L., Panić O., Wilner D., Wyatt M. C., Yelverton B., 2018, *MNRAS*, 475, 4924
- Kenyon S. J., Bromley B. C., 2002, *ApJ*, 577, L35
- Kenyon S. J., Bromley B. C., 2008, *ApJS*, 179, 451
- Kral Q., Marino S., Wyatt M. C., Kama M., Matrà L., 2019, *MNRAS*, 489, 3670
- Krivov A. V., 2010, *Res. Astron. Astrophys.*, 10, 383
- Krivov A. V., Booth M., 2018, *MNRAS*, 479, 3300
- Lee J., Song I., 2018, *MNRAS*, 475, 2955
- Lieman-Sifry J., Hughes A. M., Carpenter J. M., Gorti U., Hales A., Flaherty K. M., 2016, *ApJ*, 828, 25
- Liseau R. et al., 2008, *A&A*, 480, L47
- Liseau R. et al., 2010, *A&A*, 518, L132
- Löhne T., 2020, *A&A*, 641, A75
- Lommen D. et al., 2007, *A&A*, 462, 211
- MacGregor M. A. et al., 2013, *ApJ*, 762, L21
- MacGregor M. A., Wilner D. J., Andrews S. M., Hughes A. M., 2015a, *ApJ*, 801, 59
- MacGregor M. A., Wilner D. J., Andrews S. M., Lestrade J.-F., Maddison S., 2015b, *ApJ*, 809, 47
- MacGregor M. A. et al., 2016, *ApJ*, 823, 79
- MacGregor M. A. et al., 2017, *ApJ*, 842, 8
- MacGregor M. A. et al., 2018, *ApJ*, 869, 75
- MacGregor M. A. et al., 2019, *ApJ*, 877, L32
- Mamajek E. E., Meyer M. R., Liebert J., 2002, *AJ*, 124, 1670
- Marino S. et al., 2016, *MNRAS*, 460, 2933
- Marino S. et al., 2017, *MNRAS*, 465, 2595
- Marino S. et al., 2018, *MNRAS*, 479, 5423
- Marshall J. P. et al., 2018, *ApJ*, 869, 10
- Marshall J. P., Maddison S. T., Thilliez E., Matthews B. C., Wilner D. J., Greaves J. S., Holland W. S., 2017, *MNRAS*, 468, 2719
- Marshall J. P., Wang L., Kennedy G. M., Zeegers S. T., Scicluna P., 2021, *MNRAS*, 501, 6168
- Matrà L. et al., 2017a, *MNRAS*, 464, 1415
- Matrà L. et al., 2017b, *ApJ*, 842, 9
- Matrà L., Wyatt M. C., Wilner D. J., Dent W. R. F., Marino S., Kennedy G. M., Milli J., 2019, *AJ*, 157, 135
- Matthews B. C., Krivov A. V., Wyatt M. C., Bryden G., Eiroa C., 2014, in Beuther H., Klessen R. S., Dullemond C. P., Henning T., eds, *Protostars and Planets VI*. University of Arizona Press, Tucson, p. 521
- Matthews B. C. et al., 2015, *ApJ*, 811, 100
- Melis C., Zuckerman B., Rhee J. H., Song I., Murphy S. J., Bessell M. S., 2013, *ApJ*, 778, 12
- Moór A. et al., 2016, *ApJ*, 826, 123
- Moór A. et al., 2011, *ApJ*, 740, L7
- Moór A. et al., 2015, *ApJ*, 814, 42
- Moór A. et al., 2017, *ApJ*, 849, 123
- Moór A. et al., 2019, *ApJ*, 884, 108
- Moór A. et al., 2020, *AJ*, 159, 288
- Moro-Martín A. et al., 2015, *ApJ*, 801, 143
- Mustill A. J., Wyatt M. C., 2009, *MNRAS*, 399, 1403
- Norfolk B. J. et al., 2021, *MNRAS*, 502, 5779
- Pan M., Sari R., 2005, *Icarus*, 173, 342
- Pan M., Schlichting H. E., 2012, *ApJ*, 747, 113
- Paunzen E., 2015, *A&A*, 580, A23
- Pawellek N., Krivov A. V., 2015, *MNRAS*, 454, 3207
- Pawellek N., Krivov A. V., Marshall J. P., Montesinos B., Ábrahám P., Moór A., Bryden G., Eiroa C., 2014, *ApJ*, 792, 65
- Pecaut M. J., Mamajek E. E., 2013, *ApJS*, 208, 9
- Pecaut M. J., Mamajek E. E., Bubar E. J., 2012, *ApJ*, 746, 154
- Ricarte A., Moldvai N., Hughes A. M., Duchêne G., Williams J. P., Andrews S. M., Wilner D. J., 2013, *ApJ*, 774, 80
- Ricci L., Testi L., Maddison S. T., Wilner D. J., 2012, *A&A*, 539, L6
- Ricci L., Carpenter J. M., Fu B., Hughes A. M., Corder S., Isella A., 2015a, *ApJ*, 798, 124
- Ricci L., Maddison S. T., Wilner D., MacGregor M. A., Ubach C., Carpenter J. M., Testi L., 2015b, *ApJ*, 813, 138
- Rizzuto A. C., Ireland M. J., Robertson J. G., 2011, *MNRAS*, 416, 3108
- Sault R. J., Teuben P. J., Wright M. C. H., 1995, in Shaw R. A., Payne H. E., Hayes J. J. E., eds, *ASP Conf. Series Vol. 77, Astronomical Data Analysis Software and Systems IV*. Astron. Soc. Pac., San Francisco, p. 433
- Schneider G., Silverstone M. D., Hines D. C., 2005, *ApJ*, 629, L117
- Schüppler C. et al., 2015, *A&A*, 581, A97
- Sibthorpe B., Kennedy G. M., Wyatt M. C., Lestrade J. F., Greaves J. S., Matthews B. C., Duchêne G., 2018, *MNRAS*, 475, 3046
- Steele A., Hughes A. M., Carpenter J., Ricarte A., Andrews S. M., Wilner D. J., Chiang E., 2016, *ApJ*, 816, 27
- Su K. Y. L. et al., 2017, *AJ*, 154, 225
- Torres C. A. O., Quast G. R., da Silva L., de La Reza R., Melo C. H. F., Sterzik M., 2006, *A&A*, 460, 695
- Torres C. A. O., Quast G. R., Melo C. H. F., Sterzik M. F., 2008, *Young Nearby Loose Associations*, Vol. 2. p. 757
- Ubach C., Maddison S. T., Wright C. M., Wilner D. J., Lommen D. J. P., Koribalski B., 2012, *MNRAS*, 425, 3137
- Ubach C., Maddison S. T., Wright C. M., Wilner D. J., Lommen D. J. P., Koribalski B., 2017, *MNRAS*, 466, 4083
- Virtanen P. et al., 2020, *Nat. Methods*, 17, 261
- Williams J. P., Cieza L. A., 2011, *ARA&A*, 49, 67
- Wilner D. J., MacGregor M. A., Andrews S. M., Hughes A. M., Matthews B., Su K., 2018, *ApJ*, 855, 56
- Wilson W. E. et al., 2011, *MNRAS*, 416, 832
- Wolf S., Voshchinnikov N. V., 2004, *Comput. Phys. Commun.*, 162, 113
- Wright E. L. et al., 2010, *AJ*, 140, 1868
- Wyatt M. C., 2008, *ARA&A*, 46, 339
- Wyatt M. C., Panić O., Kennedy G. M., Matrà L., 2015, *Ap&SS*, 357, 103
- Yelverton B., Kennedy G. M., Su K. Y. L., Wyatt M. C., 2019, *MNRAS*, 488, 3588
- Zuckerman B., Song I., 2012, *ApJ*, 758, 77

APPENDIX: DEBRIS DISC SAMPLE CHARACTERISTICS

Table A1. Debris disc sample characteristics. Targets are ordered identically to Table 3 and our four new PLATYPUS sources with ATCA 8.8 mm fluxes are in bold. r_d is the outer radial extent of the dust disc. $\lambda_{1,\text{mm}}$ and $\lambda_{2,\text{mm}}$ are the flux density values referenced in Table 3.

Source	SpT	Ref.	Age (Myr)	Ref.	r_d (au)	Ref.	Dist. ^a (pc)	$\lambda_{1,\text{mm}}$ (mJy)	Ref.	$\lambda_{2,\text{mm}}$ (μ Jy)	Ref.
AU Mic	M1	1	24	1	40	15	9.72	7.14 ± 0.15	34	$>60.8 \pm 5.2$	1
CPD-72 2713	K-M	2	24	11	140	16	36.6	3.80 ± 0.59	16	95.9 ± 16.1	35
ϵ Eri	K2	1	400-800	1	69	17	41.8	17.2 ± 5.0	36	$66.1^{+6.9}_{-10.5}$	36
HD 61005	G8	1	40	1	67	18	36.4	7.2 ± 0.3	37	57.3 ± 8.6	1
HD 48370	G8	3	20-50	3	90	19	36.1	5.0 ± 0.5	35	70 ± 10.8	35
HD 107146	G2	1	80-200	1	116	20	27.4	12.5 ± 1.3	38	166.0 ± 25.2	39
HD 377	G2	1	150	1	101	21	38.5	3.5 ± 1.0	23	$< 13.1 \pm 4.4$	1
HD 105	G0	4	28	4	85	4	38.8	2.0 ± 0.4	4	42 ± 14	40
q ¹ Eri	F9	1	4800	1	85	22	17.3	39.4 ± 4.1	41	92.6 ± 16.6	39
HD 104860	F8	1	140	1	110	23	45.2	4.4 ± 1.1	23	14.0 ± 3.5	1
HD 15115	F2	1	21	1	97	24	49.0	2.6 ± 0.6	42	12.8 ± 4.1	1
HD 181327	F6	1	24	1	86	25	48.2	7.5 ± 0.1	25	145.0 ± 19.2	39
HR 8799	A5	5	30	5	232	26	41.2	3.5 ± 0.5	26	32.6 ± 9.9	26
η Crv	F2	6	1000-2000	6	152	6	18.2	9.2 ± 0.5	6	< 36	40
HD 32297	A5/6	7	15-45	12	100	18	133	3.04 ± 0.21	12	56.2 ± 16.7	35
HD 95086	A8	1	17	1	208	27	86.4	3.1 ± 0.18	27	61.9 ± 15.9	39
β Pic	A6	1	24	1	106	28	19.4	60 ± 6	43	240.0 ± 33.2	39
HD 131835	A2	8	15	8	85	29	133	8.5 ± 4.4	44	53 ± 17	40
HD 131488	A2	9	15	14	91	30	155	2.91 ± 0.31	45	59.5 ± 12.4	35
Formalhaut	A4	1	440	1	136	31	7.70	27 ± 3	46	400 ± 64	47
49 Ceti	A1	1	40	1	95	32	57.1	17 ± 3	32	25.1 ± 5.5	1
HR 4796 A	A0	10	9	5	78	33	71.9	14.4 ± 1.9	5	< 63	40

Notes. ^aDistances are taken from Gaia Collaboration (2018).

References (1) MacGregor et al. (2016), (2) Torres et al. (2006), Pecaú & Mamajek (2013), (3) Torres et al. (2008), (4) Marshall et al. (2018), (5) Holland et al. (2017), (6) Marino et al. (2017), (7) Debes et al. (2009), (8) Hung et al. (2015a), (9) Melis et al. (2013), (10) Gerbaldi et al. (1999), (11) Torres et al. (2006), Bell et al. (2015), Lee & Song (2018), Gagné et al. (2018), (12) MacGregor et al. (2018), (13) Mamajek et al. (2002), Pecaú et al. (2012), (15) Matthews et al. (2015), (16) Moór et al. (2020), (17) Booth et al. (2017), (18) MacGregor et al. (2018), (19) Moór et al. (2016), (20) Marino et al. (2018), (21) Choquet et al. (2016), (22) Liseau et al. (2010), (23) Steele et al. (2016), (24) MacGregor et al. (2019), (25) Marino et al. (2016), (26) Wilner et al. (2018), (27) Su et al. (2017), (28) Matrà et al. (2019), (29) Hung et al. (2015b), (30) Kral et al. (2019), (31) MacGregor et al. (2017), (32) Hughes et al. (2017), (33) Kennedy et al. (2018), (34) MacGregor et al. (2013; 35) this work, (36) MacGregor et al. (2015b), (37) Ricarte et al. (2013), (38) Ricci et al. (2015a), (39) Ricci et al. (2015b), (40) Marshall et al. (2017), (41) Liseau et al. (2008), (42) MacGregor et al. (2015a), (43) Dent et al. (2014), (44) Moór et al. (2015), (45) Moór et al. (2017), (46) Holland et al. (2003), and (47) Ricci et al. (2012).

This paper has been typeset from a \LaTeX file prepared by the author.